Intense Subsurface Upwelling Associated with Major Western Boundary Currents

Fanglou Liao[1], Xinfeng Liang[1*], Yun Li[1] & Michael Spall[2]

1. School of Marine Science and Policy, University of Delaware, Lewes, DE 19958, USA

2. Woods Hole Oceanographic Institution, Woods Hole, MA, 02543, USA

Abstract

Western boundary currents (WBCs) play an essential role in regulating global climate[1-5]. In contrast to their widely examined horizontal motions, less attention has been paid to vertical motions associated with WBCs. Here, we examine the vertical motions associated with the major WBCs by analyzing vertical velocity estimates from five ocean synthesis products[6-11] and one eddy-resolving ocean simulation[12]. These data reveal robust and intense subsurface upwelling in five major subtropical WBC systems. These upwelling systems are parts of basin-scale zonal overturning circulations[13, 14] and are likely driven by the meridional pressure gradients along the western boundary. The intense subsurface upwelling associated with WBCs and the basin-wide zonal overturning circulations are potentially crucial for the transport of properties and materials in the ocean interior but have long been neglected in the literature. This study suggests an overlooked role of WBCs in the climate system and showcases the usefulness of ocean vertical velocity estimates from various data products.

* Corresponding author (email: xfliang@udel.edu)

Introduction

Large-scale vertical motion in the global ocean is generally much weaker than horizonal motions[15], yet vertical transport is crucial in both the climate and biogeochemical systems. For instance, upwelling near the surface brings nutrient-enriched water into the euphotic zone, affecting the ocean primary productivity[16, 17] and, consequently, CO_2 uptake[18-20]. Downwelling, such as that observed in the Southern Ocean, transports heat and tracers sourced at the surface to the deep and abyssal oceans[21-23], and is therefore essential for the responses of the ocean interior to changes in climate and human activities[21].

Based on theoretical understanding (e.g., Ekman dynamics) and the observed distributions of a variety of tracers[24], a number of general patterns of ocean vertical motions have been inferred, including strong upwelling along the eastern boundaries of the subtropical ocean basins and along the equator[17, 25, 26], as well as intense vertical motions of both signs in the Southern Ocean[25, 27]. However, because the weak vertical velocity associated with the large-scale circulations cannot, in general, be measured directly with existing instruments, studies of vertical motions are limited, especially in the subsurface ocean. Some available ocean data products, especially ocean state estimates and ocean reanalyses[28, 29] constrained by observations, provide estimates of ocean vertical velocity. Once proven robust, such data products can complement existing observations and advance our quantitative understanding of large-scale vertical motions in the global ocean.

The vertical motions associated with WBCs and their impacts on subsurface vertical exchanges have not been studied widely. Despite the fact that all major WBCs, including the Gulf Stream and Kuroshio, are three-dimensional features, their role in the climate system has long been

studied in terms of lateral transport and air-sea exchange[30], largely neglecting the effects of vertical motions. In fact, regional observations[31] and the long-term mean vertical velocity field from a global ocean state estimate[32] have revealed considerable vertical motions associated with the WBCs, even in the absence of local upwelling-favorable wind stress. Such WBC-associated vertical motions potentially offer a viable and effective mechanism for the exchange of ocean heat, salt, and other biogeochemical tracers between the upper ocean and the underlying water masses over long timescales.

In this study, we examine estimates of vertical velocity in the major WBC regions from one ocean state estimate (ECCO v4r3[10, 11]), four ocean reanalyses (ECMWF ora-s3[6]; GODAS[7]; SODA 3.4.2[8]; ECDA[9]) and one eddy-resolving ocean simulation (OFES[12]) over their overlapping period (January 1992 to December 2009). Our primary goals are to describe and explain robust large-scale features of vertical motions in the WBC regions and to explore their roles in the vertical transport of water masses and ocean properties. In order to demonstrate differences between vertical motions near eastern and western boundaries of ocean basins, we also include the Peruvian upwelling region as a contrasting example.

Results

Subsurface vertical velocity associated with the major WBCs. Time-averaged vertical velocity $\bar{w}$ near 300 m from six selected ocean products is displayed in Fig. 1. While there are differences in the detailed regional patterns, intense vertical motions in the Southern Ocean, along the Equator, and in the WBC regions are observed in all of the examined data products. In contrast to the strong $\bar{w}$ in the Southern Ocean[33] and in the equatorial regions[34], which are mainly induced by Ekman dynamics, the strong and robust upwelling (~1 m/day) apparent in the WBC

regions in all six products is less well understood. Also, both the strength and vertical extent of the upwelling in the WBC regions are distinctly different from those in the eastern boundary upwelling systems, the latter of which are barely detectable at this depth. Strong upwelling can be also seen at 1000 m and deeper in WBC regions, especially near the Gulf Stream and the Kuroshio (Supplementary Figs. 1-2). Apart from the boundary current systems, the vast area of the subtropical oceans at this depth is dominated by weak downwelling.

We also present selected sections of the time-averaged vertical velocity $\overline{\boldsymbol{w}}$ across the major WBCs from ECCO (Fig. 2). Despite differences in resolutions, numerical configurations, and assimilated data, all of the examined products show similar spatial patterns (Supplementary Figs. 3-8). Intense subsurface upwelling in the WBC regions is collocated with the strong boundary currents, suggesting a dynamical connection between them. Also, the strong time-averaged upwelling (~1 m/day) in WBC regions generally extends from near the surface down to 1000 m or even deeper. The strong vertical motion is, however, located well above the bottom topography, suggesting that it does not result from direct interaction with the sloping bottom. In contrast to the WBC sections, upwelling near the Peruvian coast, in a sample eastern boundary upwelling region, is confined to a shallower layer and is also much weaker. Furthermore, weak downwelling with various vertical extents occurs to the east of the WBC upwelling, suggesting possible zonal overturning circulations in the subtropical ocean basins.

Basin-wide zonal overturning and WBC upwelling. In order to confirm the existence of the zonal overturning circulation suggested above and to examine its relationship with WBC upwelling, we examine the time-averaged velocities in the plane of zonal sections ($\overline{\boldsymbol{u}}$, $\overline{\boldsymbol{w}}$) averaged within the latitudinal bands marked in Fig. 1b. Zonal overturning circulations are prominent in the North Pacific, North Atlantic and in the Indian Ocean (Fig. 3). Despite

differences in detailed structure, all the zonal overturning circulations show weak downward currents inside the ocean basins and strong upwelling near the western boundaries. The intense subsurface upwelling in the WBC regions is, therefore, part of the zonal overturning circulation in the subtropical ocean basins. Note that while this two-dimensional view of a zonal overturning circulation is useful for visualization, it must be kept in mind that the flow is three dimensional[35, 36] and time dependent.

The existence of zonal overturning circulations in subtropical ocean basins has been demonstrated in previous studies based on idealized numerical simulations[13, 14]. Meridional gradients in surface buoyancy forcing can drive eastward flows in the upper ocean and westward flows at intermediate depths through the thermal wind balance. Due to mass conservation, upwelling and downwelling are expected at the western and eastern boundaries, respectively, to close the loop. Our analysis shows that similar zonal overturning circulations also exist in realistic settings, as they appear both in a high-resolution realistic numerical simulation (OFES) and in several coarse-resolution ocean synthesis data products. We infer that zonal overturning circulations with upwelling in WBCs are not just theoretical predictions but likely real features of the ocean.

In order to seek additional evidence for upwelling in WBC regions, we conduct a few regional analyses. The relationship between the current vectors and the background (zonal) density structure is first examined. Figure 3 shows that velocity vectors in the WBC regions are approximately aligned with sloping isopyncal surfaces associated with the WBCs, suggesting that the strong upwelling in the WBC regions is primarily along rather than across isopycnals. In other words, the strong WBC upwelling is unlikely to be related to local mixing, by which vertical velocity will be primarily in diapycnal direction instead of along isopycnals. A

111 decomposition of the vertical velocity[37] from ECCO into diapycnal and isopycnal contributions
112 confirms that the WBC upwelling is mainly associated with along-isopycnal flow
113 (Supplementary Fig. 9). The potential density in the upper 1000 m in the ECCO data increases in
114 the poleward direction along all WBCs (Fig. 4) due to heat loss at the surface and lateral eddy
115 fluxes. The resulting meridional density gradients are balanced by the vertical shear of the zonal
116 velocity (Figs. 2 and 3), as expected from thermal wind. It is this change in stratification along
117 the western boundaries that provides the large-scale constraint for the observed upwelling in the
118 WBCs.

119 The underlying relationship between vertical stratification, horizontal transport, and upwelling is
120 illustrated through a sample volume budget analysis for the Gulf Stream (Fig. 5). The surface
121 area of the control volume is triangular and marked in the inset, and the depth range is between
122 55 m and 2000 m. The budget analysis (Fig. 5a) reveals large horizontal divergences below 300
123 m, requiring vertical transport to conserve mass. The density structure along the two sections
124 (BA, BC in Fig. 5b) provides a dynamical explanation for the existence of horizontal
125 convergence. Since the density increases poleward along the western boundary (Fig. 4), the
126 density change from the western boundary to the interior point (B) is larger along the northern
127 section (BC) than it is along the southern section (AB). Thermal wind thus requires a larger
128 vertical shear in the horizontal velocity along BC. But mass conservation requires that the flow
129 through each section is the same (except for the small transport into the upper 55 m). The only
130 way to close the mass budget is for water to upwell within the control volume. Similar upwelling
131 is found for an idealized high resolution numerical experiment in which a current is cooled with
132 the coast on the left side[38]. In other words, the WBC upwelling can be explained through mass

conservation and geostrophy. The requirement that there be upwelling near the western boundary is not dependent on the details of the numerical model, subgrid mixing, or bottom topography.

Vertical transport associated with the WBC upwelling. We now quantify the contribution of the WBC upwelling to the vertical transport of mass/volume in the subtropical ocean basins using ECCO (Fig. 6), with the other products generally showing similar results (Supplementary Figs. 3-8). Although the WBC regions occupy only a minor portion of the subtropical ocean basins with respect to the ocean surface area, as shown in Fig. 1b, the vertical volume transport induced by upwelling in the WBCs is generally of the same order of magnitude as and is almost always opposite in the direction to the vertical volume transport in the rest of the subtropical basin within the same latitudinal band. Again, this result is consistent with the conclusion that the WBC upwelling is part of the zonal overturning circulation in the subtropical ocean basins. We also calculate the vertical transport of heat and salt using ECCO (Supplementary Figs. 10-11), and the results are consistent with the volume transport, that the WBC regions dominate subsurface vertical transport of salt and heat in the subtropical ocean basins within certain depth ranges.

Specifically, the upwelling in the Kuroshio, Gulf Stream, and Brazil Current regions dominates the net volume transport in the corresponding subtropical ocean basins within the depth ranges between a few hundred and about 2000 m. As a contrasting example, vertical volume transport in the Peruvian upwelling region is much weaker and shallower compared to the WBC upwelling. The net volume transport in the subtropical basin is in general downward near the surface and changes to upward beneath, reflecting the fact that the upward volume transport in the WBCs generally reaches its maximum around 200-500 m. In contrast, the downward transport in the rest of the subtropical basins has its maximum downward volume transport near the surface. The

surface intensified downwelling is due to the Ekman pumping occurring inside the subtropical ocean basins and that the maximum impact of the Ekman pumping generally appears around 100 m and then decreases significantly with increasing depth, as expected from Sverdrup dynamics. Also, the finding that the zonal overturning circulation is not closed within these latitude bands emphasizes that the WBC upwelling is part of a basin-scale three-dimensional overturning circulation[35, 36], part of this upwelling is balanced by downwelling at higher latitudes.

We also calculate and compare the vertical volume transport associated with the four major upwelling regimes (WBCs, Eastern Boundary Currents, Equator and Southern Ocean) around the global ocean with ECCO (Fig. 7). Near the surface, equatorial upwelling is the dominant process for the global oceanic vertical volume transport, with a maximum value around 100 Sv. But in the subsurface, the strongest upward transport is associated with the Southern Ocean and the WBC regions. Between 200 m and 1000 m, the WBC-related upward volume transport is generally more than 1/3 of the value in the Southern Ocean, with the maximum value around 25 Sv appearing near 400 m. Below 2000 m the pressure gradient along the western boundary is weak and thus a reduced contribution to the upward transport is expected. Again, this comparison confirms that the overlooked role of the WBC upwellings in the subsurface vertical exchanges of ocean properties and materials.

Discussion

To the best of our knowledge, this is the first study providing convincing evidence for the existence of as well as a dynamical explanation for intense subsurface upwelling associated with the major WBCs around the global ocean. Vertical motions in many regions of the global ocean, such as in Eastern Boundary Currents, along the Equator, and in the Southern Ocean, show

178 evident upwelling signals in surface temperature and/or chlorophyll fields[17, 24-27, 39] and have
179 been known and studied for a long time. In contrast, vertical motions in WBC regions are
180 generally weak at the surface and only become strong below the surface. Also, the strong
181 horizontal transport and eddies associated with WBCs make direct detection of surface signals of
182 WBC upwelling challenging. The intense subsurface upwelling in WBC regions, therefore, have
183 long been unrecognized in the literature.

184 Although in this study subsurface upwelling in the WBC regions is not directly measured but
185 from a variety of ocean data products, there is evidence supporting the inference that WBC
186 upwelling is likely a real phenomenon in the global ocean. The primary reason we believe that
187 the WBC upwelling is real is that in order for the western boundary currents to remain in
188 geostrophic balance to leading order, the observed density gradient along the western boundary
189 requires that there be upwelling. Secondly, the WBC subsurface upwelling appears in all the
190 examined products (Supplementary Figs. 3-8), including coarse-resolution ocean synthesis
191 products and a high-resolution ocean model simulation. Those products differ in many aspects,
192 including ocean model numerics, external forcing, mixing parameterizations and assimilated
193 observational data. The apparent robustness of WBC upwelling suggests that it is likely
194 controlled by a mechanism that is well represented in all the products. Thirdly, vertical motions
195 in other regions of the global ocean (e.g., at low latitudes, and in eastern boundary currents) in
196 the examined data products are generally consistent with previous theoretical and observational
197 studies, further increasing our confidence in their representation of the large-scale vertical
198 motions. Finally, previous idealized theoretical and numerical model studies suggest the
199 existence of zonal overturning circulations in the subtropical ocean basins. Although this aspect
200 has never been explicitly examined, those zonal overturning circulations have upwelling

branches near the western boundaries. Our finding of subsurface WBC upwelling is therefore consistent with the predictions of those prior studies.

This basic mechanism of the WBC upwelling is analogous to the dynamics of the downwelling limb of the buoyancy-forced meridional overturning circulation[38, 40], where the Eulerian downwelling is located in regions of density gradients along the boundary. Eddies contribute an important buoyancy flux which allows parcels to flow along rising isopycnals while the mean Eulerian transport would imply a large downward diapycnal flux[40, 41]. We expect that eddies may also be important in WBCs but anticipate a lesser role than in downwelling regions because the Eulerian vertical velocity is of the same sign as the flow along rising isopycnals whereas for downwelling they are of opposite sign.

Since vertical motions in the WBC regions can reach much deeper than in equatorial and Eastern Boundary upwelling, and may also extend upward into the surface mixed layer, they can play an important role in the subsurface exchange of ocean properties and materials and air-sea exchange in the subtropical regions. Given the consistent and strong vertical motions, the vertical transport of heat and carbon in the WBCs may be significant in regulating the heat and carbon content in both the upper ocean and atmosphere over longer timescales. Moreover, the basin-wide zonal overturning circulations in the subtropical ocean basins could exchange ocean properties and tracers between the ocean interior and western boundaries, as well as playing a role in the climate system.

Our results showcase the use of estimates of ocean vertical velocity. While point-wise estimates of ocean vertical velocity from models and reanalysis products are generally weak and noisy, spatial filtering reveals interesting and robust large-scale patterns that are not readily apparent in

other variables. We consider it particularly surprising that we have been able to determine a novel aspect of WBCs, one of the most widely studied ocean processes, simply by examining estimates of time-averaged vertical velocity from available ocean synthesis and modeling products. At present, few ocean synthesis products and climate models provide output of ocean vertical velocity, which we suggest should be archived routinely.

Methods

Data. Estimates of vertical velocity from six publicly available datasets, including one ocean state estimate, four ocean reanalyses, and one eddy-resolving ocean simulation, were analyzed in this study. Some basic information on those datasets is provided in the following. The ECCO (Estimating the Circulation and Climate of the Ocean) data utilized in this study are the ECCOv4r3 monthly estimates[10, 11]; ECDA is the Ensemble Coupled Data Assimilation System developed at the Geophysical Fluid Dynamics Laboratory[9]; ECMWF used here is ECMWF ora-s3, an operational ocean analysis/reanalysis system implemented at the ECMWF (European Centre for Medium-Range Weather Forecasts[6]); GODAS is the Global Ocean Data Assimilation operated at the National Centers for Environmental Prediction[7]; SODA used here is the version 3 of the Simple Ocean Data Assimilation that is based on the ocean component of the coupled CM2.5 model maintained at NOAA/GFDL[8], and the SODA data we used are monthly interpolated values; OFES is an eddy-resolving quasi-global ocean model developed by the Japan Agency for Marine-Earth Science and Technology[12].

For consistency, all available vertical velocity estimates from the six products were transformed to the LLC90[10] (Lat-Lon-Cap 90) grid before further processing. A 3 grids × 3 grids smoothing

filter included in the gcmfaces[10] package was applied to obtain robust large-scale patterns. Other smoothing filters (2 × 2, 4 × 4) were also tested, and the results were roughly the same. Additional information about the data products can be found in the Supplementary Table 1.

Domain of the WBC and Peruvian upwelling regions. As shown in Fig 1a, we define a box for each subtropical WBC region and for the Peruvian upwelling region. The regions covered by those boxes are as follows: Kuroshio, (120°E, 28°N) to (150°E, 40°N); Gulf Stream, (82°W, 25°N) to (60°W, 41 ° N); Agulhas Current, (20°E, 37°S) to (38°E, 27 °S); East Australian Current, (148°E, 37°S) to (158°E, 20°S); Brazil Current, (56°W, 35°S) to (30°W, 10°S); Peruvian upwelling, (85 ° W, 40 ° S) to (70 ° W, 8 ° S).

Global distribution of time-averaged vertical velocity $\bar{w}$. The overlapping period covered by all six products is from Jan 1992 to Dec 2009. The vertical velocity data were averaged over this 18-years period. We include three sample layers (50 m, 300 m, and 1000 m) here and show the layer around 300 m in the main text and the other two layers in the supplementary information. For each of the six data products, we use the vertical layer closest to the three nominal depths.

Vertical structure of time-averaged vertical motions in WBCs. For each WBC region, we choose a cross section approximately perpendicular to the local coastline and plot the distribution of time-averaged vertical velocity along with the horizontal velocity that is in the plane of the cross section. Details of the selected cross sections are as follows: Kuroshio, (139°E, 35°N) to (149°E, 25°N); Gulf Stream, (74°W, 38°N) to (64°W, 28°N); Agulhas Current, (30°E, 31°S) to (40°E, 41°S); East Australian Current, (153°E, 30°S) to (163°E, 30°S); and Brazil Current, (41°W, 21°S) to (31°W, 21°S). A contrasting eastern boundary upwelling, the Peruvian upwelling

region, was also selected from (70°W, 23°S) to (80°W, 23°S). The cross sections are marked in Fig. 1a.

Zonal overturning circulation. For the domains represented by the black boxes in Fig. 1b, we calculate meridionally averaged vertical and zonal velocities, which are normalized to the regional horizontal and vertical maxima, respectively, for better visualization. The maxima of depth in each longitude line within the box is added, taken from the General Bathymetric Chart of the Oceans, is shown in Fig. 3.

Vertical velocity decomposition. Vertical velocity at the sample depth (300 m) is decomposed into isopycnal and diapycnal components following previous studies[37]. Firstly, potential density is calculated with temperature and salinity data from ECCO; secondly, the horizontal isopycnal slopes in the east-west and north-south directions are calculated; thirdly, isopycnal velocity is calculated by using the continuity equation in density coordinates, and diapycnal velocity is calculated based on the principle that the diapycnal mixing contributes to the advective part of any potential density sources in the diapycnal direction.

Volume budget analysis. We choose the Gulf Stream region as an example and calculate the horizontal time-averaged volume transport at the two lateral sides and also the time-averaged vertical volume transport through the upper and bottom surfaces. The depths of the upper and bottom surfaces are chosen so that the vertical volume transport at the upper surface is below the Ekman layer and that at the bottom surface is relatively weak. Note that the ECCO data on the native grid are used for the budget analysis.

Vertical volume, heat and salt transport. At each depth layer, we select the grids with positive mean vertical velocity and calculate the upward vertical volume flux in the domain bounded by

each box in Fig. 1a. We define the results as the vertical volume transport related to the WBC upwelling. We also calculate the volume transport within all the other grid cells in the same latitude band across the whole ocean basin (domain shown in Fig. 1b). The sum of these two terms is the net volume transport within the corresponding latitude band across the ocean basin. The vertical heat flux is obtained by multiplying the vertical velocity with specific heat and temperature at each grid, and then integrating in the same way as the volume transport. Note that we use normalized temperature by dividing the temperature of each grid by the global mean temperature in the corresponding vertical layer, to account for the large vertical gradient in temperature. To calculate the vertical salt transport, we multiply the vertical velocity with salinity at each grid and integrate them in the same way as for the vertical volume transport.

Comparison of the vertical volume transport associated with different upwelling regimes. We calculate the vertical volume transport at each grid where the time-averaged vertical velocity is positive in all the four different regimes: WBC, Eastern Boundary Current, Equator (within 8° equator toward) and the Southern Ocean (south to 40°S). Note that the Angola Dome is classified into the eastern boundary current region in this paper. These upward volume transports are then summed over the corresponding region and compared with each other.

Code availability. The scripts used to make the plots in this paper are available from the corresponding author on request.

Data Availability. All the data used in this study are publicly available. The ECCOv4r3 data are available at https://ecco.jpl. nasa.gov/products/all/. The ECDA data are available at ftp://nomads.gfdl.noaa.gov/2/ECDA/ecda/GFDL-CM2.1-ECDA/CM2.1R-ECDA-v3.1-

1960/mon/ocean/dc_Omon/r1i1p1/v20110601/. The ECMWF data are available at http://apdrc.soest.hawaii.edu:80/dods/public_data/Reanalysis_Data/ORA-S3/1x1_grid. The GODAS data are available at http://apdrc.soest.hawaii.edu:80/dods/public_data/Reanalysis_Data/GODAS/monthly. The SODA data are available at https://www.atmos.umd.edu/~ocean/index_files/soda3.4.2_mn_download_b.htm. The OFES data are available at http://www.jamstec.go.jp/esc/fes/dods/ OFES/OFES_NCEP_RUN. The bathymetry data are available at https://www.gebco.net/data_and_products/gridded_bathymetry_data/.

Reference

1. Stommel, H.M. The Gulf Stream. A Physical and Dynamical Description. (Cambridge University Press, 1965)

2. Imawaki, S., Bower, A. S., Beal, L. & Qiu, B. Western boundary currents. *Ocean Circulation and Climate - A 21st Century Perspective*. G. Siedler et al., Eds., Academic Press. **103**, 305-338 (2013).

3. Minobe, S., et al. Influence of the Gulf Stream on the troposphere. *Nature* **452**, 206-209 (2008).

4. Takahashi, T., et al. Climatological mean and decadal change in surface ocean pCO2, and net sea–air CO2 flux over the global oceans. *Deep-Sea Res. Part II: Topical Studies in Oceanography* **56**, 554-577 (2009).

5. Wu, L., et al. Enhanced warming over the global subtropical western boundary currents. *Nat. Climate Change* **2**, 161-166 (2012).

6. Balmaseda, M.A., Vidard, A. & Anderson, D.L. The ECMWF ocean analysis system: ORA-S3. *Mon. Weather. Rev.* **136**, 3018-3034 (2008).

7. Behringer, D. & Xue, Y. Evaluation of the global ocean data assimilation system at NCEP: The Pacific Ocean. *Proc. Eighth Symp. on Integrated Observing and Assimilation Systems for Atmosphere, Oceans, and Land Surface*. 2004. AMS 84th Annual Meeting, Washington State Convention and Trade Center.

8. Carton, J.A., Chepurin, G.A. & Chen, L.SODA3: A new ocean climate reanalysis. *J. Clim.* **31**, 6967-6983 (2018).

9. Chang, Y.-S., et al. An assessment of oceanic variability for 1960–2010 from the GFDL ensemble coupled data assimilation. *Clim. Dyn.* **40**, 775-803 (2013).

10. Forget, G., Campin, J.M., Heimbach, P., Hill, C.N., Ponte, R.M. and Wunsch, C. ECCO version 4: an integrated framework for non-linear inverse modeling and global ocean state estimation, *Geosci. Model Dev.,* **8**, 3071–3104 (2015)

11. Fukumori, I., et al. ECCO version 4 release 3. http://hdl.handle.net/1721.1/110380 (2017).

12. Sasaki, H., et al.. An eddy-resolving hindcast simulation of the quasiglobal ocean from 1950 to 2003 on the Earth Simulator. *High resolution numerical modelling of the atmosphere and ocean*. 157-185 (2008).

13. Bryan, F. Parameter sensitivity of primitive equation ocean general circulation models. *J. Phys. Oceanogr.* **17**, 970-985 (1987).

14. Cessi, P., Wolfe, C.L. & Ludka, B.C. Eastern-boundary contribution to the residual and meridional overturning circulations. *J. Phys. Oceanogr.* **40**, 2075-2090 (2010).

15. Stewart, R.H. Introduction to physical oceanography. 2008: Texas A & M University College Station.

16. Ryther, J.H. Photosynthesis and fish production in the sea. *Science* **166**, 72-76 (1969).

17. Kämpf, J. & Chapman, P. Upwelling systems of the world. 2016: Springer.

18. Ducklow, H.W., Steinberg, D.K. & Buesseler, K.O. Upper ocean carbon export and the biological pump. *Oceanography* **14**, 50-58 (2001).

19. Pilskaln, C.H., et al. Carbon export and regeneration in the coastal upwelling system of Monterey Bay, central California. *J. Mar. Res.* **54**, 1149-1178 (1996).

20. Stukel, M.R., et al. Contributions of mesozooplankton to vertical carbon export in a coastal upwelling system. *Mar. Ecol. Prog. Ser.* **491**, 47-65 (2013).

21. Gregory, J.M. Vertical heat transports in the ocean and their effect on time-dependent climate change. *Clim. Dyn.* **16,** 501-515 (2000).

22. Ito, T., Woloszyn, M. & Mazloff, M. Anthropogenic carbon dioxide transport in the Southern Ocean driven by Ekman flow. *Nature* **463**, 80–83 (2010).

23. Liang, X., et al. Vertical redistribution of oceanic heat content. *J. Clim.* **28**, 3821-3833 (2015).

24. Toggweiler, J., et al. Upwelling in the ocean basins north of the ACC: 1. on the upwelling exposed by the surface distribution of $\Delta^{14}C$. *J. Geophys. Res. -Oceans.* **124**, 2591-2608 (2019).

25. Huyer, A. Coastal upwelling in the California Current system. *Prog. Oceanogr.* **12**, 259-284 (1983).

26. Wyrtki, K. An estimate of equatorial upwelling in the Pacific. *J. Phys. Oceanogr.* **11**, 1205-1214 (1981).

27. Marshall, J. & Speer, K. Closure of the meridional overturning circulation through Southern Ocean upwelling. *Nat. Geosci.* **5**, 171-180 (2012).

28. Stammer, D., et al. Ocean data assimilation in support of climate applications: status and perspectives. *Ann. Rev. Mar. Sci.* **8**, 491-518 (2016).

29. Balmaseda, M.A., et al. The ocean reanalyses intercomparison project (ORA-IP). *J. Oper. Ocenograph.* **8**, S80-S97 (2015).

30. Hu, D., et al. Pacific western boundary currents and their roles in climate. *Nature* **522**, 299-308 (2015).

31. Roughan, M. and Middleton, J.H. On the East Australian Current: variability, encroachment, and upwelling. *J. Geophys. Res. -Oceans.* **109**, C7 (2004).

32. Liang, X., Spall, M. & Wunsch, C. Global ocean vertical velocity from a dynamically consistent ocean state estimate. *J. Geophys. Res. -Oceans.* **122**, 8208-8224 (2017).

33. Anderson, R., et al. Wind-driven upwelling in the Southern Ocean and the deglacial rise in atmospheric CO2. *Science* **323**, 1443-1448 (2009).

34. Yoshida, K. A Theory of the cromwell current (the equatorial undercurrent) and of the equatorial upwelling: an interpretation in a similarity to a costal circulation. *日本海洋学会誌* **15**, 159-170 (1959).

35. Talley, L.D. Shallow, intermediate, and deep overturning components of the global heat budget. *J. Phys. Oceanogr.* **33**, 530-560 (2003).

36. Boccaletti, G., et al. The vertical structure of ocean heat transport. *Geophys. Res. Lett.* **32**, L10603, doi:10.1029/2005GL022474 (2005).

37. Bennett, S.L. The relationship between vertical, diapycnal, and isopycnal velocity and mixing in the ocean general circulation. *J. Phys. Oceanogr.* **16**, 167-174 (1986).

38. Katsman, C.A., et al. Sinking of dense north atlantic waters in a global ocean model: location and controls. *J. Geophys. Res. -Oceans.* **123**, 3563-3576 (2018).

39. Naveira Garabato, A.C., et al. High-latitude ocean ventilation and its role in Earth's climate transitions. *Phil. Trans. R. Soc. A.* **375**, 20160324 (2017).

40. Spall, M.A. Buoyancy-forced downwelling in boundary currents. *J. Phys. Oceanogr.,* **38,** 2704-2721 (2008).

41. Cessi, P. & Wolfe, C.L. Adiabatic eastern boundary currents. *J. Phys. Oceanogr.* **43**, 1127-1149 (2013).

Acknowledgments

X.L. is supported by the National Science Foundation through Grant OCE-2021274 and the Alfred P. Sloan Foundation through Grant FG-2019-12536. M.A.S is supported through the National Science Foundation Grant OCE-1947290. Comments from Carl Wunsch, Young-Oh Kwon and Jinbo Wang on an early version of this paper are helpful. We also greatly appreciate comments and edits from Andreas Thurnherr on various versions of this paper.

Author contributions

X.L. and Y.L. conceived the study. F.L. conducted the analyses. M.A.S. helped to develop the mechanistic explanation. X.L. and F.L. drafted the manuscript. All authors discussed the results and contributed to improving the manuscript.

Competing interests

The authors declare no competing interests.

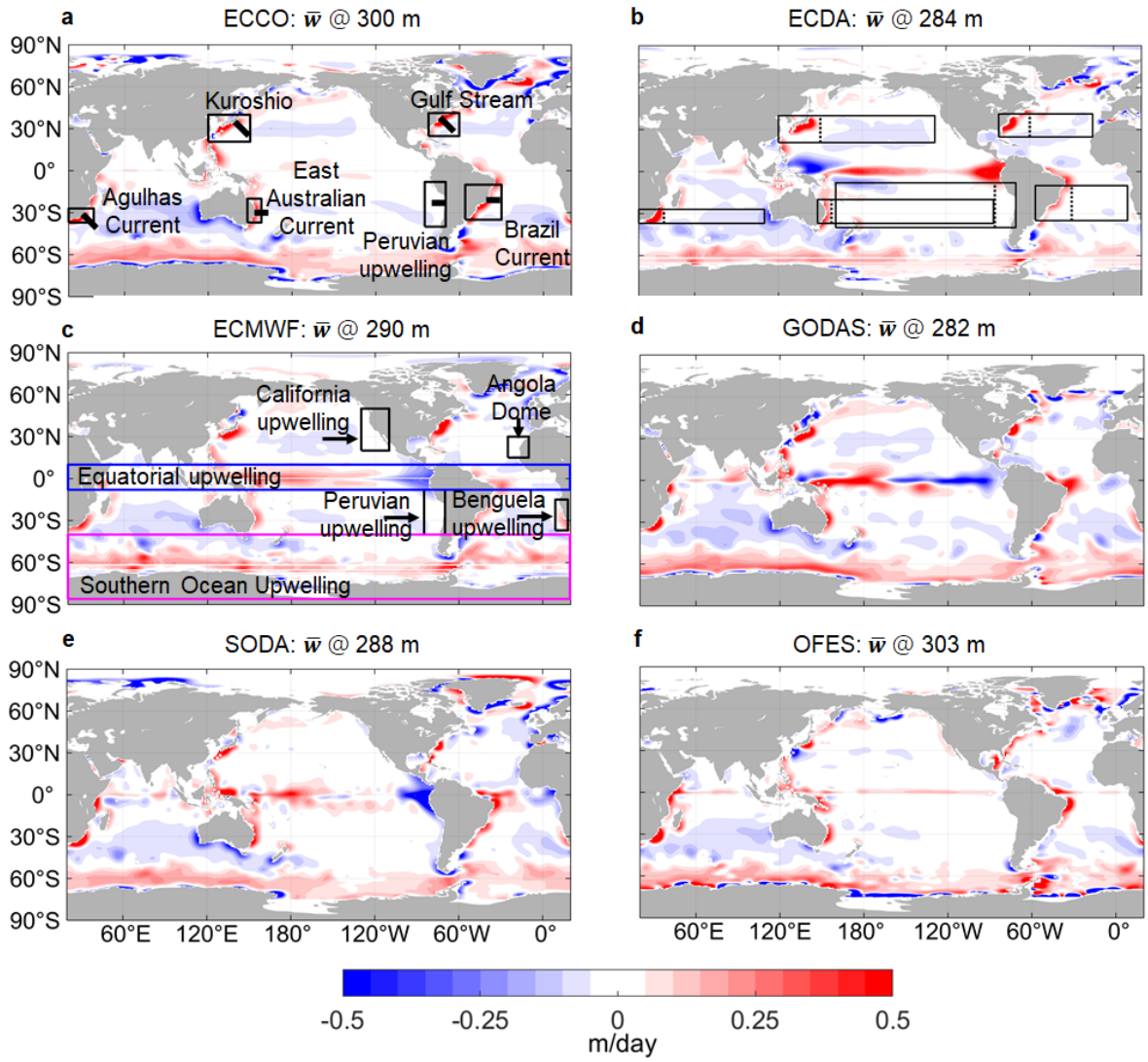

424

425 **Fig. 1** Time-averaged vertical velocity $\bar{w}$ near 300 m between Jan 1992 and Dec 2009. $\bar{w}$ from
426 six selected products: **a** ECCO. **b** ECDA. **c** ECMWF. **d** GODAS. **e** SODA. **f** OFES. The black
427 boxes in **a** show the domains of the five western boundary and one eastern boundary systems
428 investigated in this study. The thick black lines represent the cross sections shown in Fig. 2. The
429 black boxes in **b** (at the same latitude band of the corresponding boxes in **a**) represent the
430 domains where vertical volume flux was calculated. The dashed lines roughly split the domains
431 into WBC regions and the rest of the subtropical ocean basins. Boxes in **c** mark three other well-
432 known upwelling regimes (equatorial, eastern boundary and the Southern Ocean).

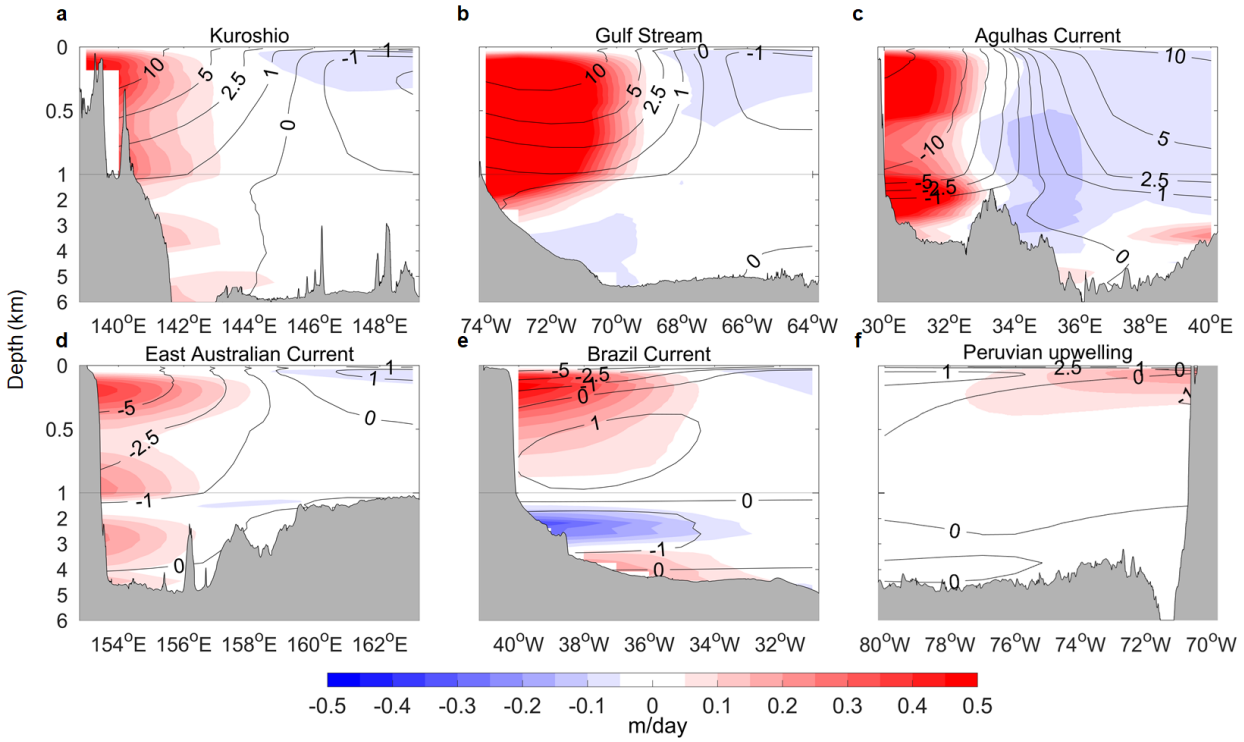

433

434 **Fig. 2** Time-averaged vertical velocity $\bar{w}$ (colour) and horizontal velocity (contour lines, unit:

435 cm/s) in selected cross sections from ECCO. The other datasets show similar spatial patterns

436 (Supplementary Figs. 3-8). The cross sections are marked with black lines in Fig. 1a. **a** Kuroshio.

437 **b** Gulf Stream. **c** Agulhas Current. **d** East Australian Current. **e** Brazil Current. **f** Peruvian

438 upwelling. The contour lines show the horizontal velocity (cm/s) perpendicular to the cross

439 sections, indicative of the strength of adjacent western boundary currents. Note that the depth

440 axis is stretched for better visualization.

441

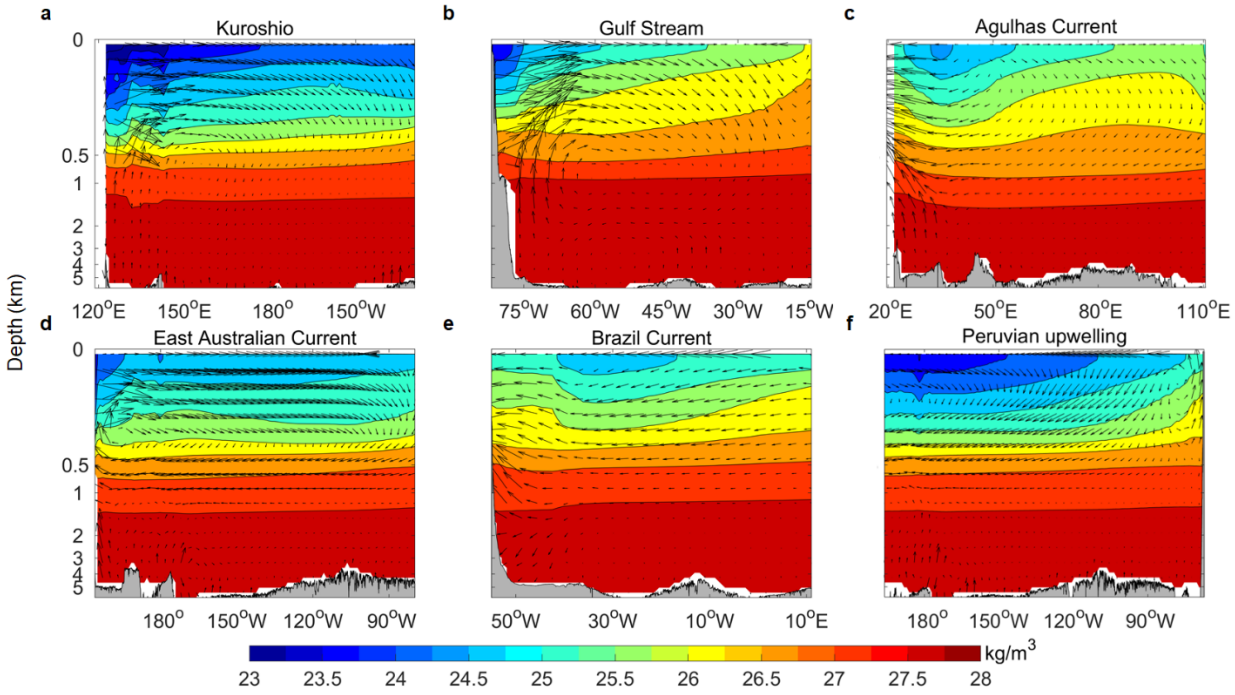

442

443 **Fig. 3** Meridional averages of the time-averaged current vector (arrows, normalized in each
444 region individually for better visualization) and potential density anomaly (contours) in selected
445 regions from ECCO. The other datasets show similar spatial patterns. The averaged regions,
446 which are marked with black boxes in Fig. 1b, correspond to: **a** Kuroshio. **b** Gulf Stream. **c**
447 Agulhas Current. **d** East Australian Current. **e** Brazil Current. **f** Peruvian upwelling.

448

449

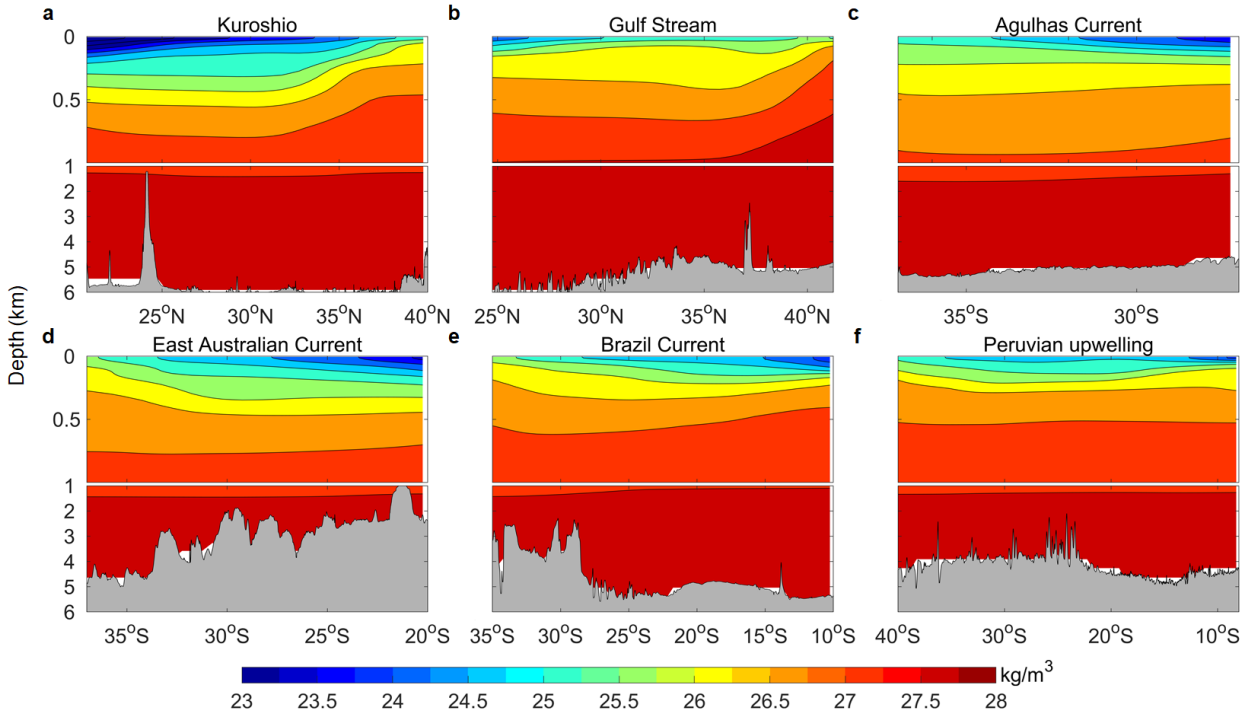

450

451 **Fig. 4** Potential density along the WBCs and Peruvian upwelling. The potential density

452 anomalies were derived along the meridional direction of the WBC regions marked in Fig. 1. **a**

453 Kuroshio. **b** Gulf Stream. **c** Agulhas Current. **d** East Australian Current. **e** Brazil Current. **f**

454 Peruvian upwelling.

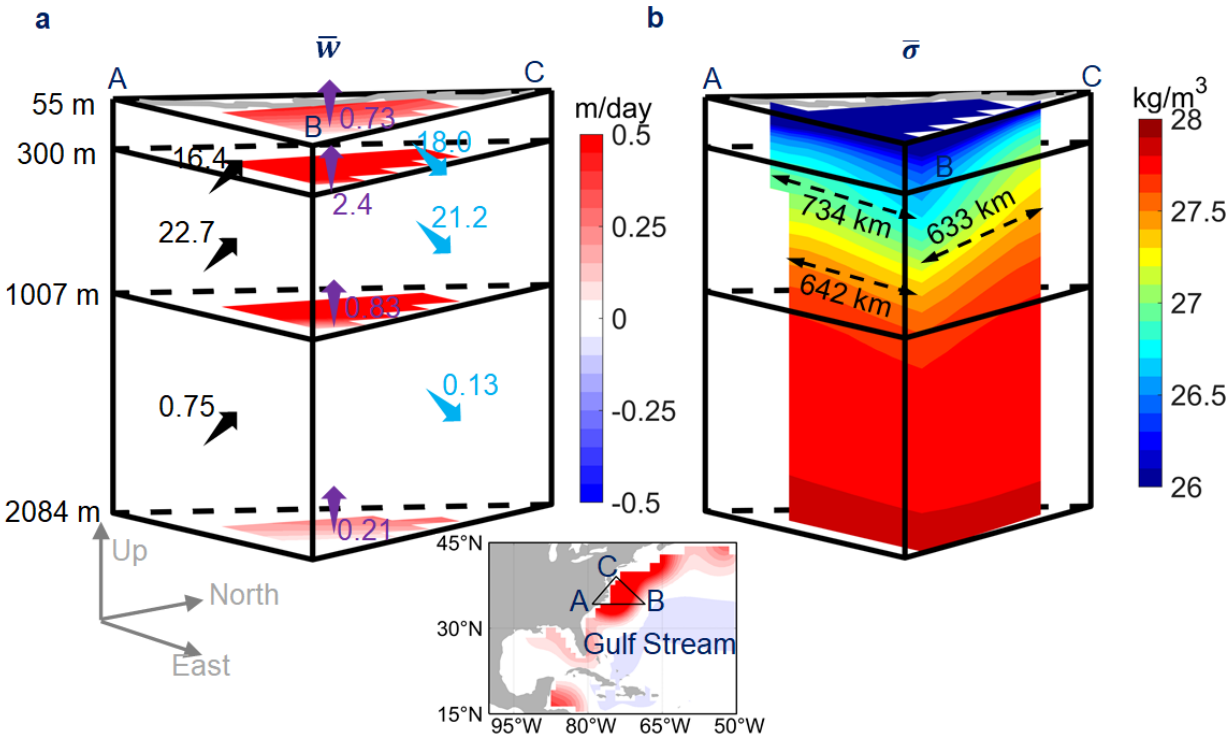

455

456 **Fig. 5** Time-averaged vertical velocity $\bar{w}$, potential density anomaly $\bar{\sigma}$, and volume flux in a
457 triangle-shape domain in the Gulf Stream region. **a** Time-averaged vertical velocity at four
458 depths (colours) and lateral and vertical volume fluxes. The black and blue arrows represent the
459 lateral volume fluxes in Sv, and the purple arrows show the vertical volume fluxes in Sv. **b**
460 Time-averaged potential density anomaly along the sections AB and BC of the triangle-shaped
461 domain between 55 and 2000 m (shown in the inset). The grey curve in the 55 m section in **a, b**
462 represents the coastline. The results are based on ECCO data on the native grids.

463

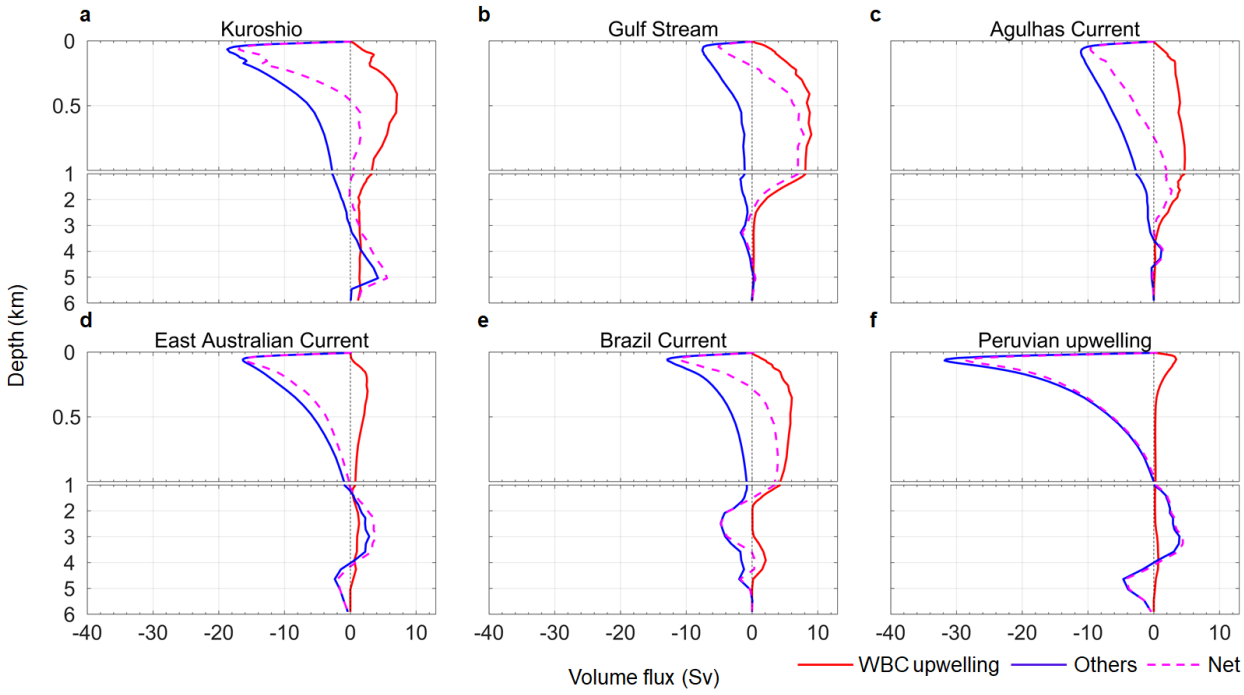

464

465 **Fig. 6** Vertical volume fluxes in the subtropical ocean basins from ECCO. Vertical volume
466 transport due to the WBC upwelling is shown in red, vertical volume transport integrated across
467 the rest of the corresponding ocean basin within the same latitude band is shown in blue, and the
468 net vertical volume transport is displayed as the magenta dashed line. The six regions, which are
469 marked in Fig. 1b, correspond to **a** Kuroshio. **b** Gulf Stream. **c** Agulhas Current. **d** East
470 Australian Current. **e** Brazil Current. **f** Peruvian upwelling. Note that the depth axis is divided
471 into two parts for better visualization.

472

473

474

475

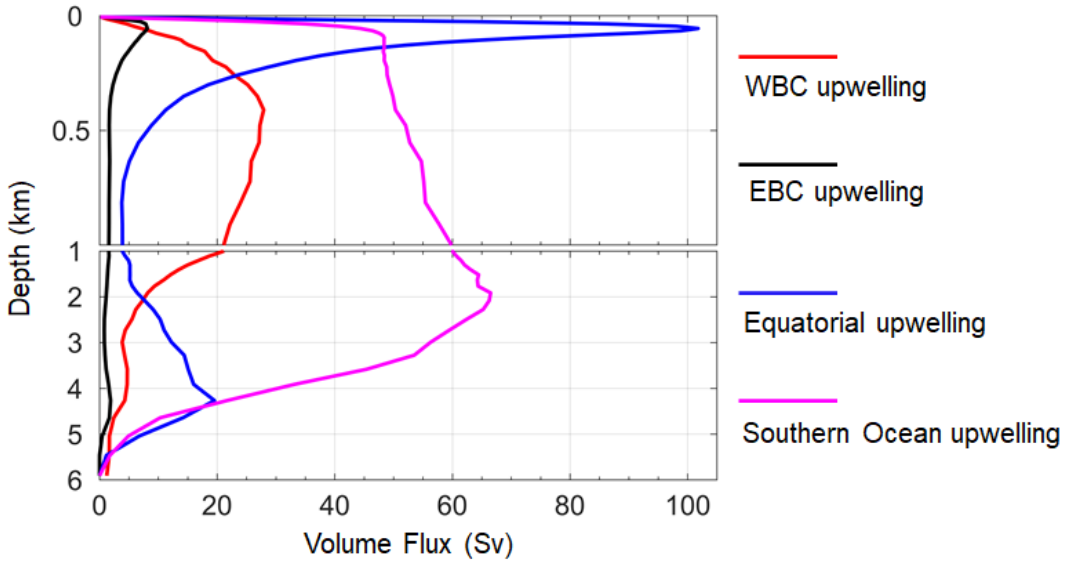

476

477 **Fig. 7** Comparisons of vertical volume transport in four different upwelling regimes. The four
478 regimes are WBCs, the Eastern Boundary Currents (EBC), the Equatorial region and the
479 Southern Ocean. The vertical volume transport is calculated within the corresponding upwelling
480 regions marked in Fig. 1c.

481

Supplementary Information for

Intense Subsurface Upwelling Associated with Major Western Boundary Currents

Fanglou Liao[1], Xinfeng Liang[1*], Yun Li[1] & Michael Spall[2]

1. School of Marine Science and Policy, University of Delaware, Lewes, DE 19958, USA

2. Woods Hole Oceanographic Institution, Woods Hole, MA, 02543, USA

Supplementary Figures

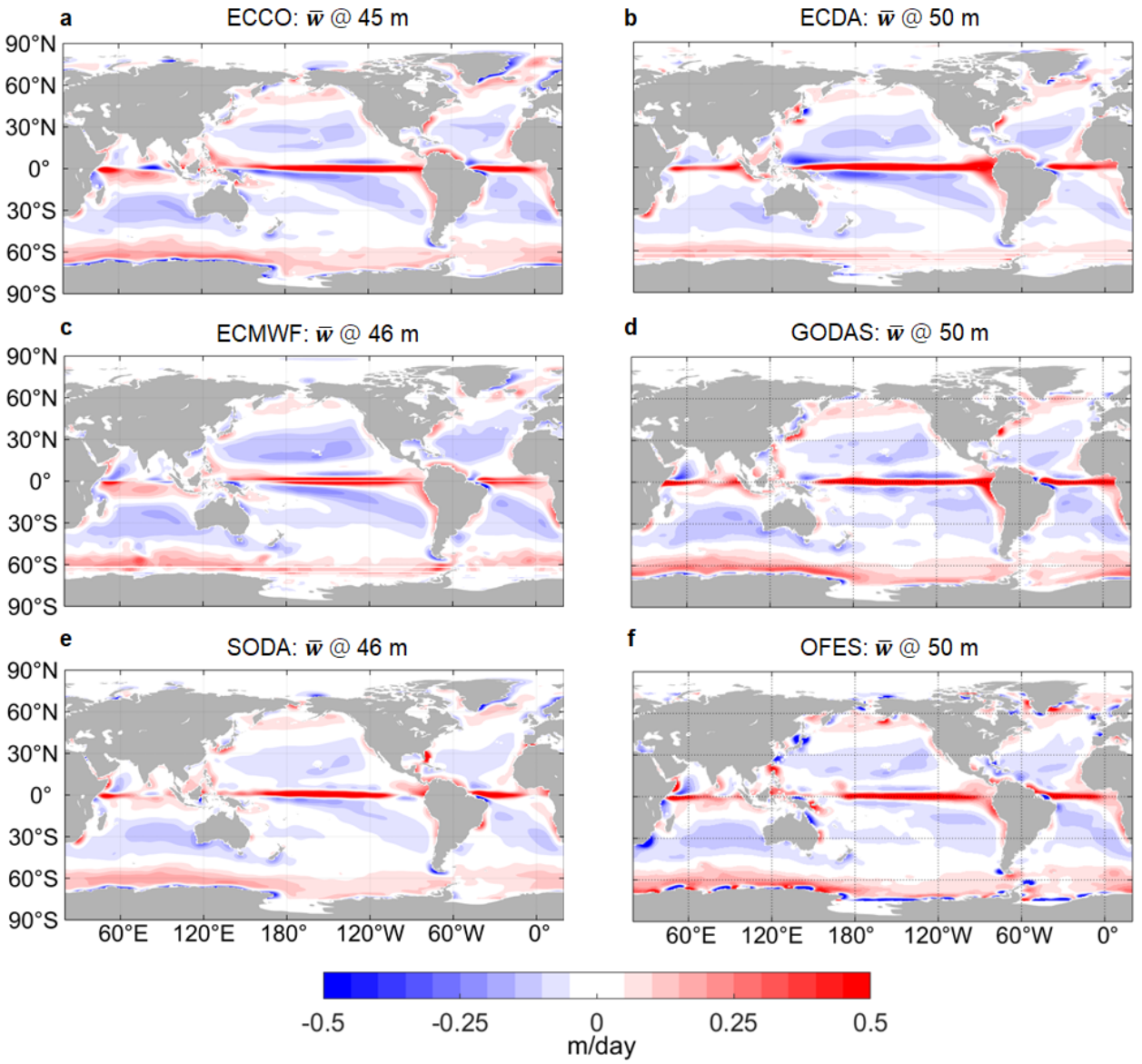

Supplementary Fig. 1 Time-averaged vertical velocity $\overline{w}$ at around 50 m. **a** ECCO. **b** ECDA. **c** ECMWF. **d** GODAS. **e** SODA. **f** OFES.

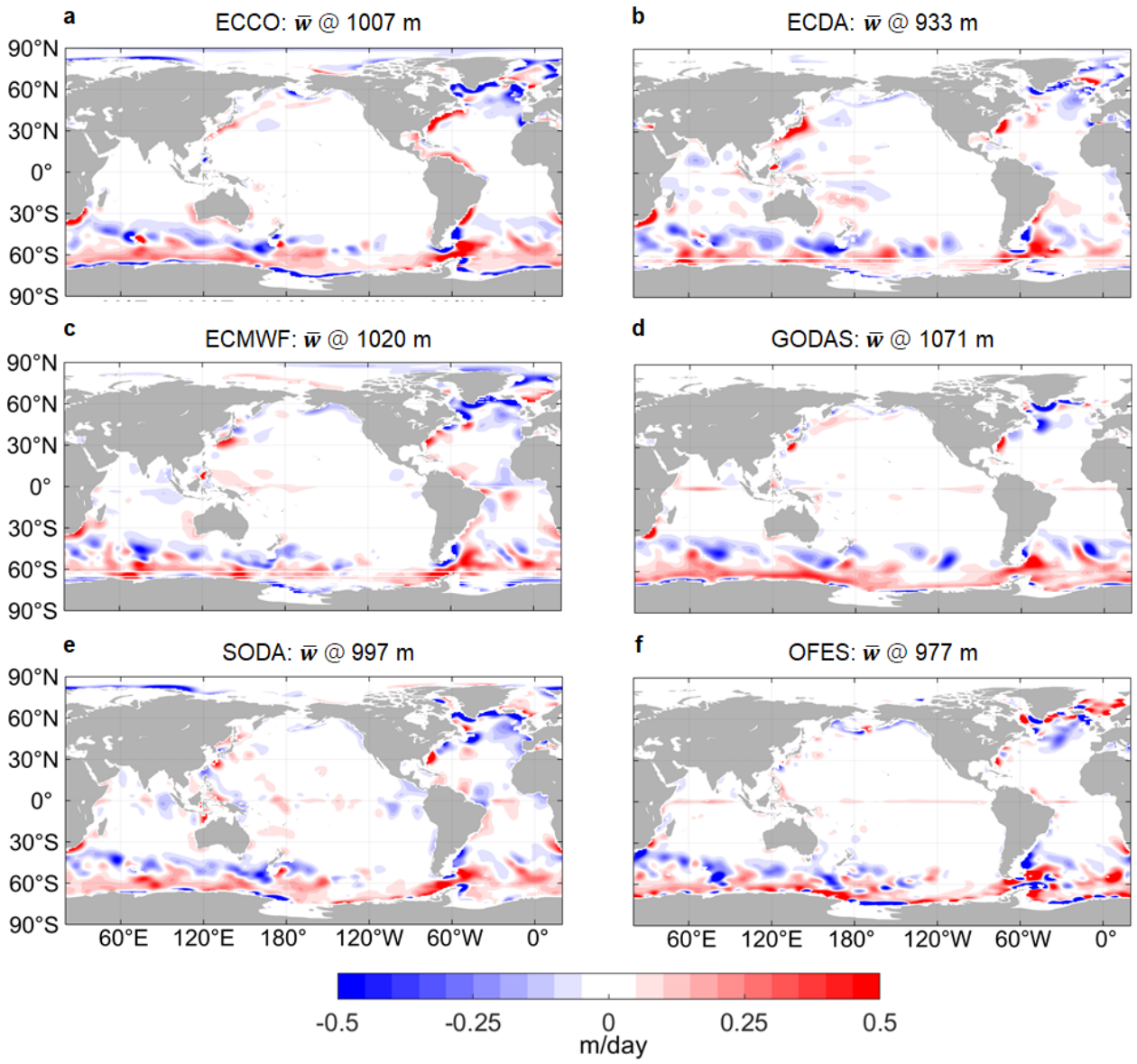

507

508 **Supplementary Fig. 2** Time-averaged vertical velocity $\bar{w}$ at around 1000 m. **a** ECCO. **b** ECDA.

509 **c** ECMWF. **d** GODAS. **e** SODA. **f** OFES.

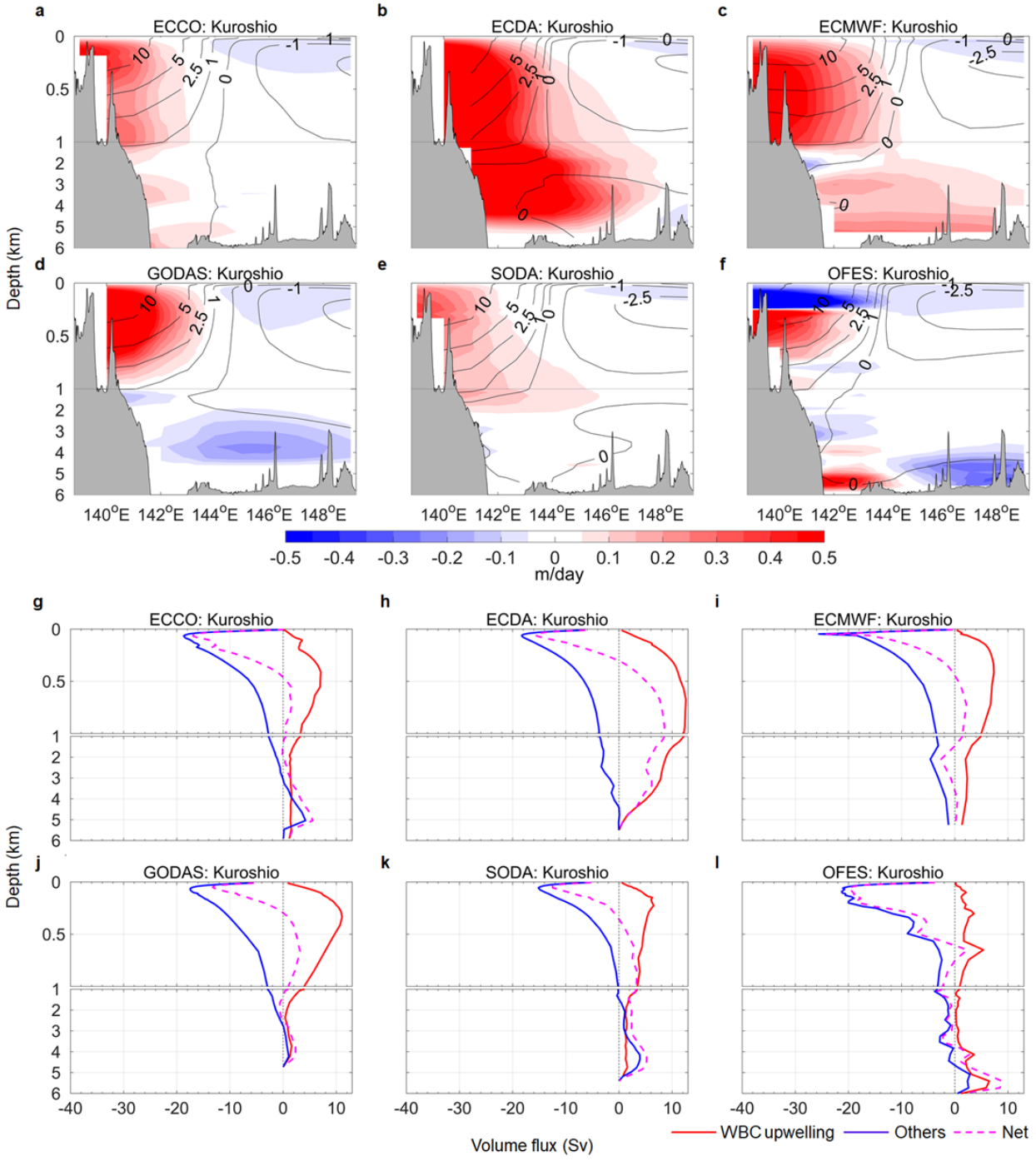

510

511 **Supplementary Fig. 3** Time-averaged vertical velocity $\overline{w}$ (colour) along with horizontal speed

512 distribution (contours, unit: cm/s) in selected cross sections (shown in Fig. 1a) and volume flux

513 in the Kuroshio Current region. **a, g** ECCO. **b, h** ECDA. **c, i** ECMWF. **d, j** GODAS. **e, k** SODA.

514 **f, l** OFES.

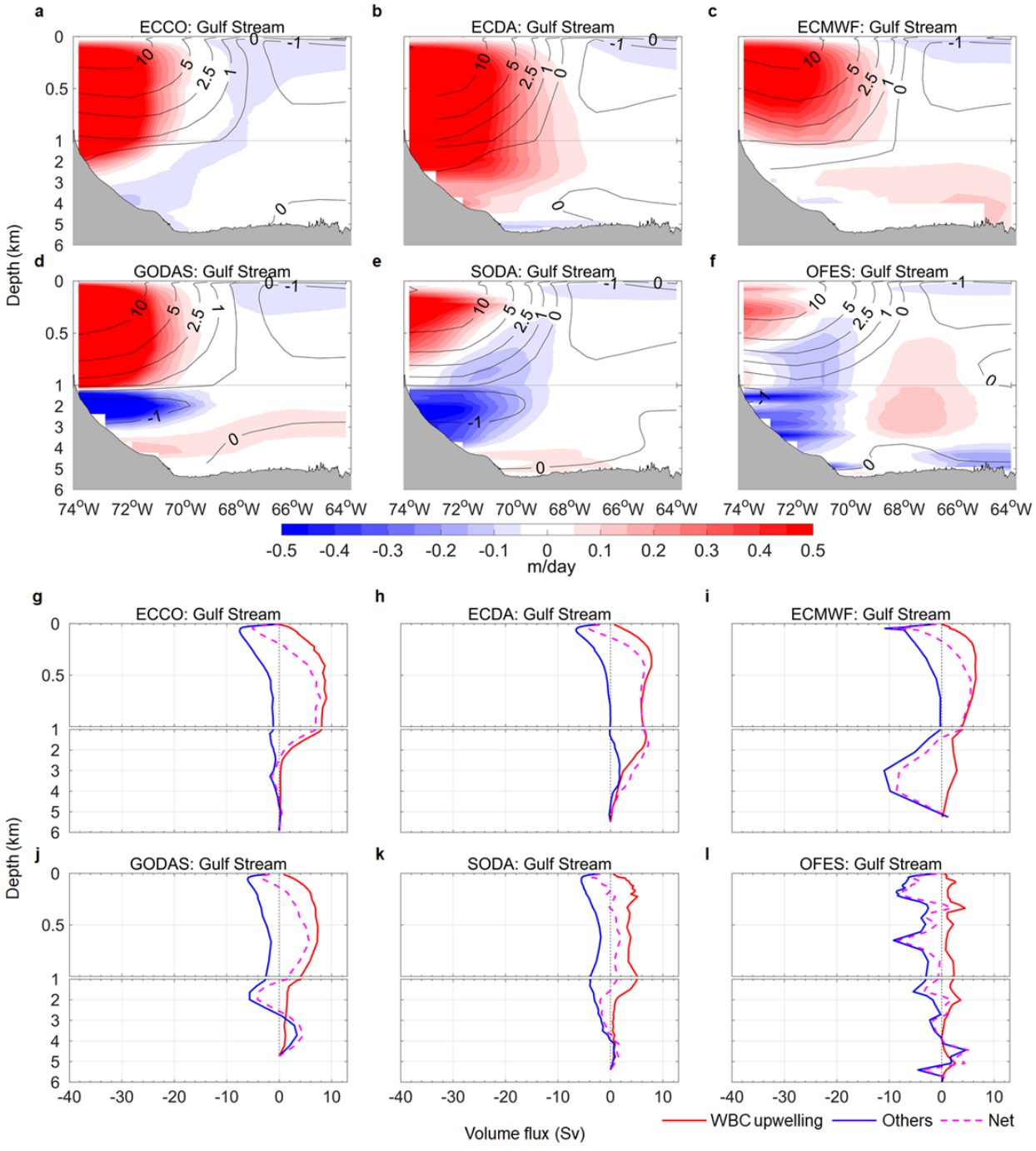

515

516 **Supplementary Fig. 4** Time-averaged vertical velocity $\overline{w}$ (colour) along with horizontal speed

517 distribution (contours, unit: cm/s) in cross sections (shown in Fig. 1a) and volume flux in the

518 Gulf Stream region. **a, g** ECCO. **b, h** ECDA. **c, i** ECMWF. **d, j** GODAS. **e, k** SODA. **f, l** OFES.

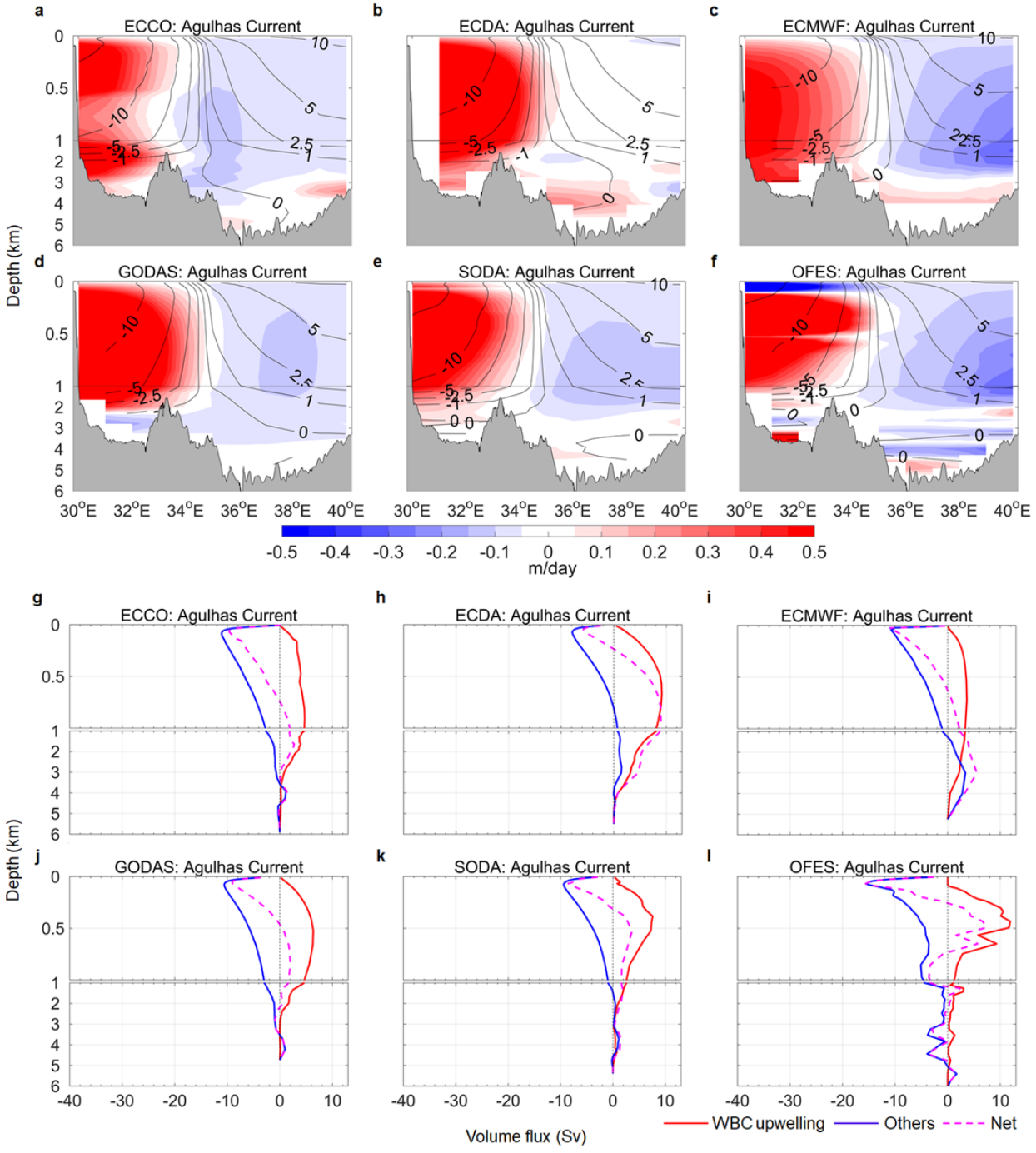

519

520 **Supplementary Fig. 5** Time-averaged vertical velocity $\overline{w}$ (colour) along with horizontal speed

521 distribution (contours, unit: cm/s) in cross sections (shown in Fig. 1a) and volume flux in the

522 Agulhas Current region. **a, g** ECCO. **b, h** ECDA. **c, i** ECMWF. **d, j** GODAS. **e, k** SODA. **f, l**

523 OFES.

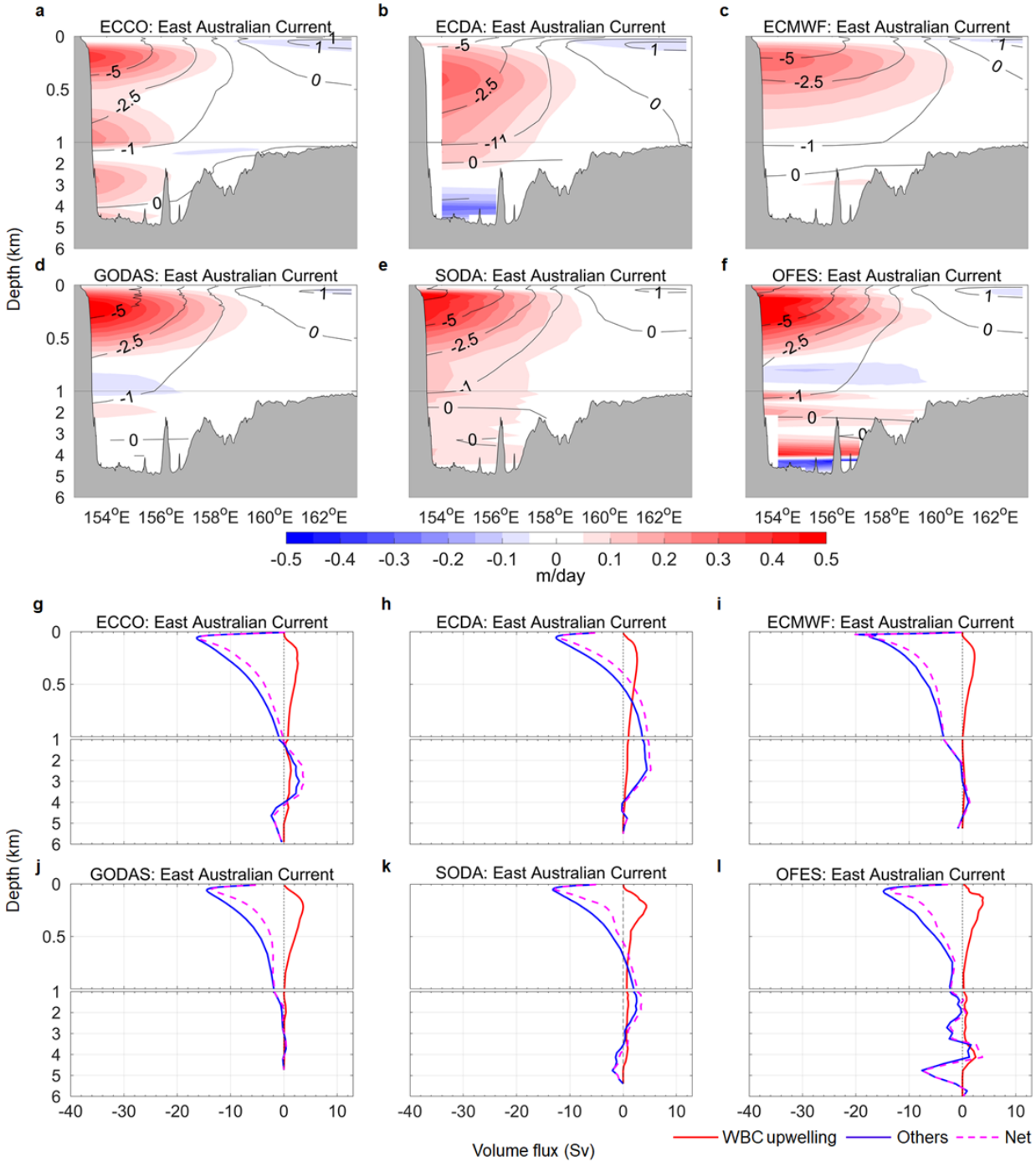

524

525 **Supplementary Fig. 6** Time-averaged vertical velocity $\overline{w}$ (colour) along with horizontal speed

526 distribution (contours, unit: cm/s) in cross sections (shown in Fig. 1a) and volume flux in the

527 East Australian Current region. **a, g** ECCO. **b, h** ECDA. **c, i** ECMWF. **d, j** GODAS. **e, k** SODA.

528 **f, l** OFES.

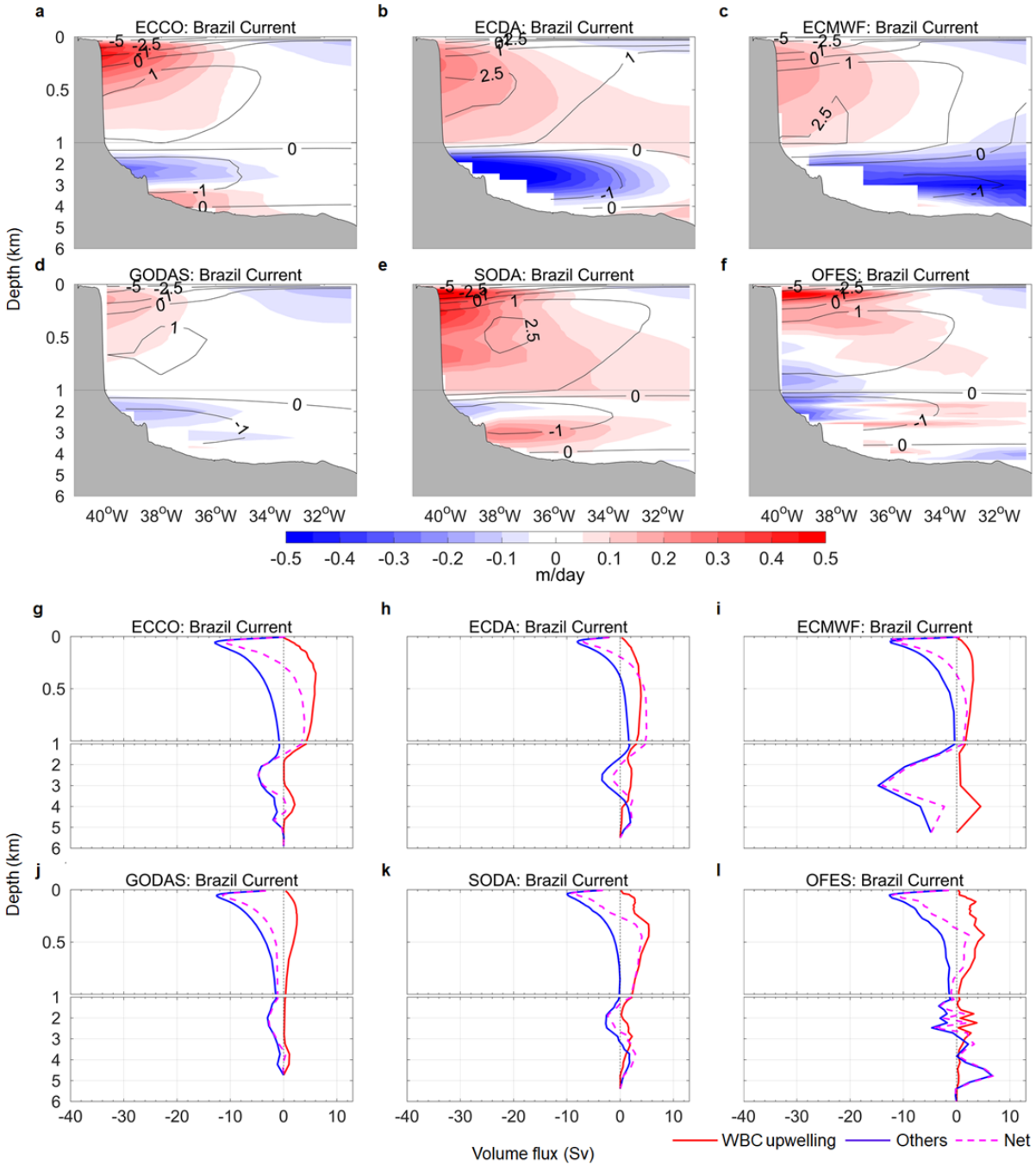

529

530 **Supplementary Fig. 7** Time-averaged vertical velocity $\overline{w}$ (colour) along with horizontal speed

531 distribution (contours, unit: cm/s) in cross sections (shown in Fig. 1a) and volume flux in the

532 Brazil Current region. **a, g** ECCO. **b, h** ECDA. **c, i** ECMWF. **d, j** GODAS. **e, k** SODA. **f, l**

533 OFES.

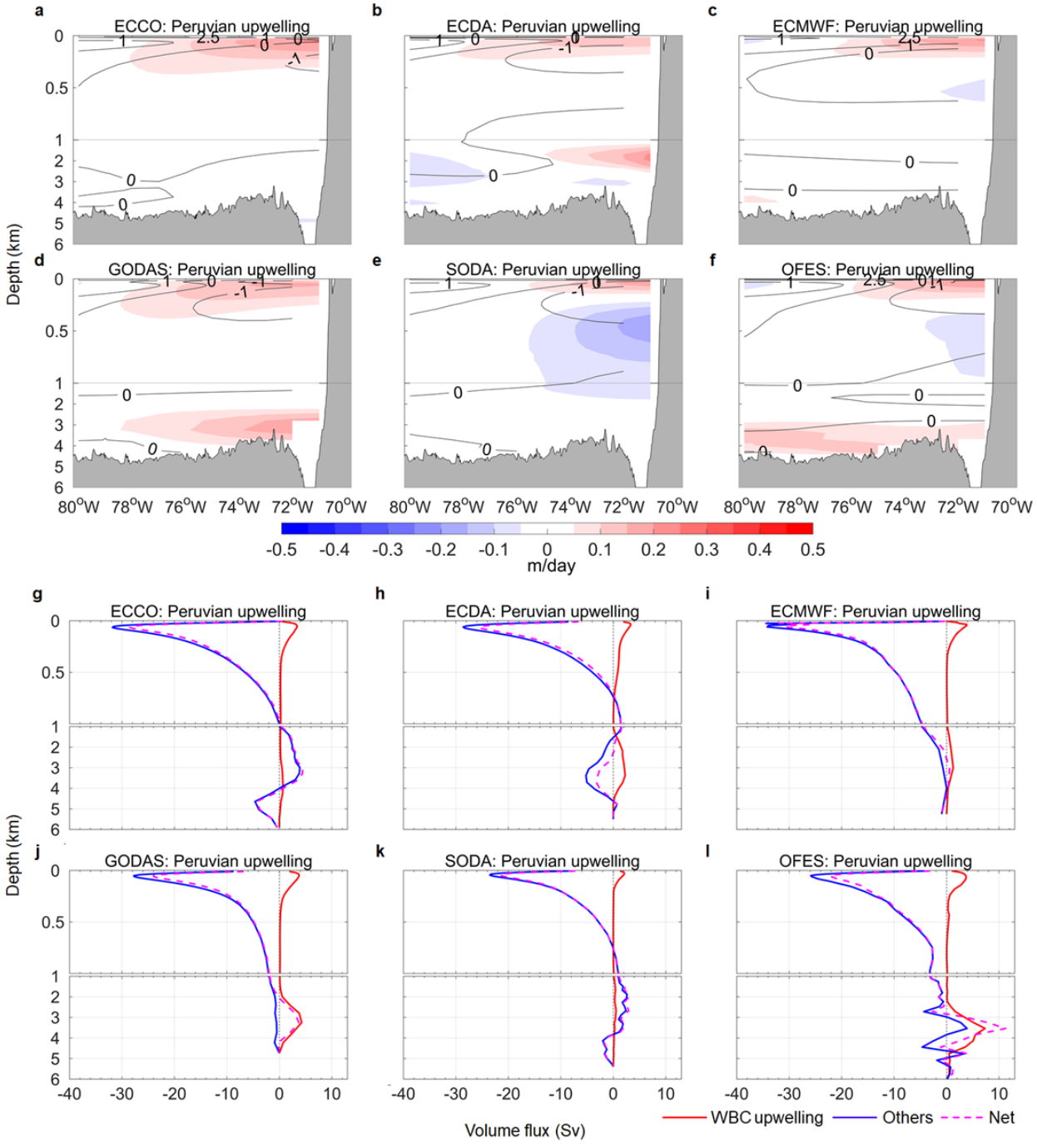

534

535 **Supplementary Fig. 8** Time-averaged vertical velocity $\overline{w}$ (colour) along with horizontal speed

536 distribution (contours, unit: cm/s) in cross sections (shown in Fig. 1a) and volume flux in the

537 Peruvian upwelling region. **a, g** ECCO. **b, h** ECDA. **c, i** ECMWF. **d, j** GODAS. **e, k** SODA. **f, l**

538 OFES.

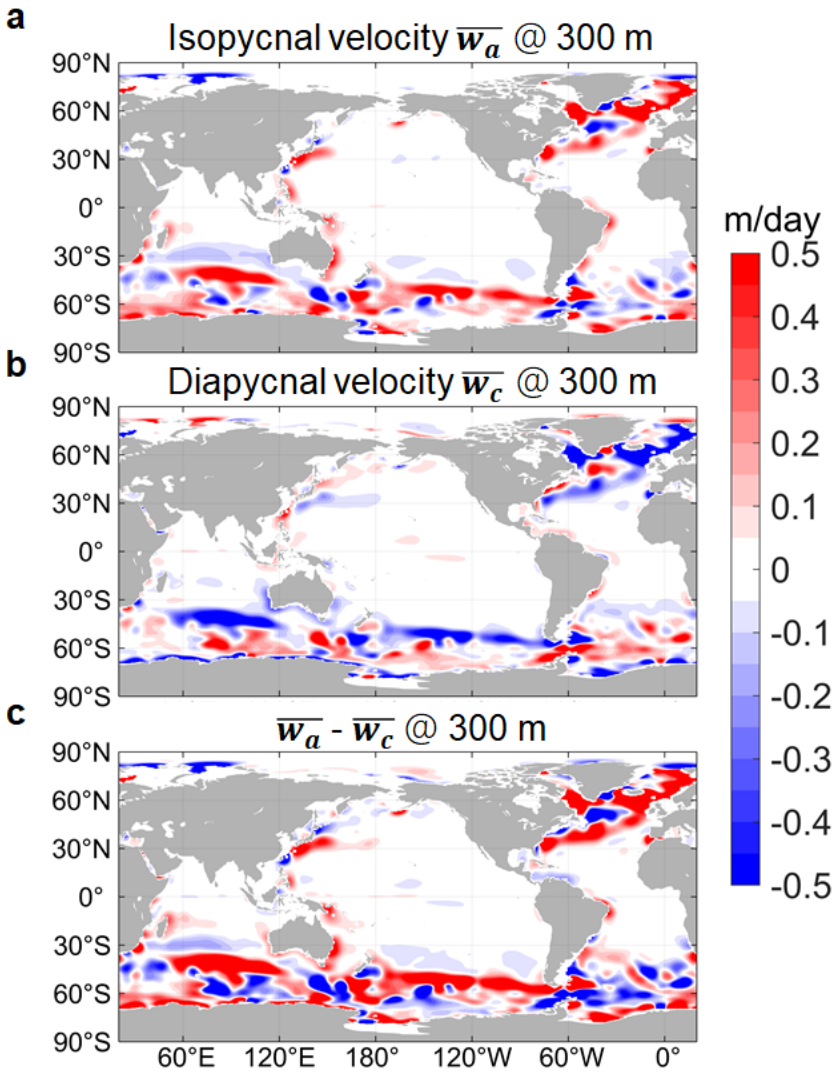

539

540 **Supplementary Fig. 9** Along- and across-isopycnal components of the time-mean vertical

541 velocity $\overline{w}$ at around 300 m. **a** Isopyncal vertical velocity. **b** Diapycnal vertical velocity. **c**

542 Differences between isopyncal and diapycnal vertical velocities. The results are based on ECCO.

543

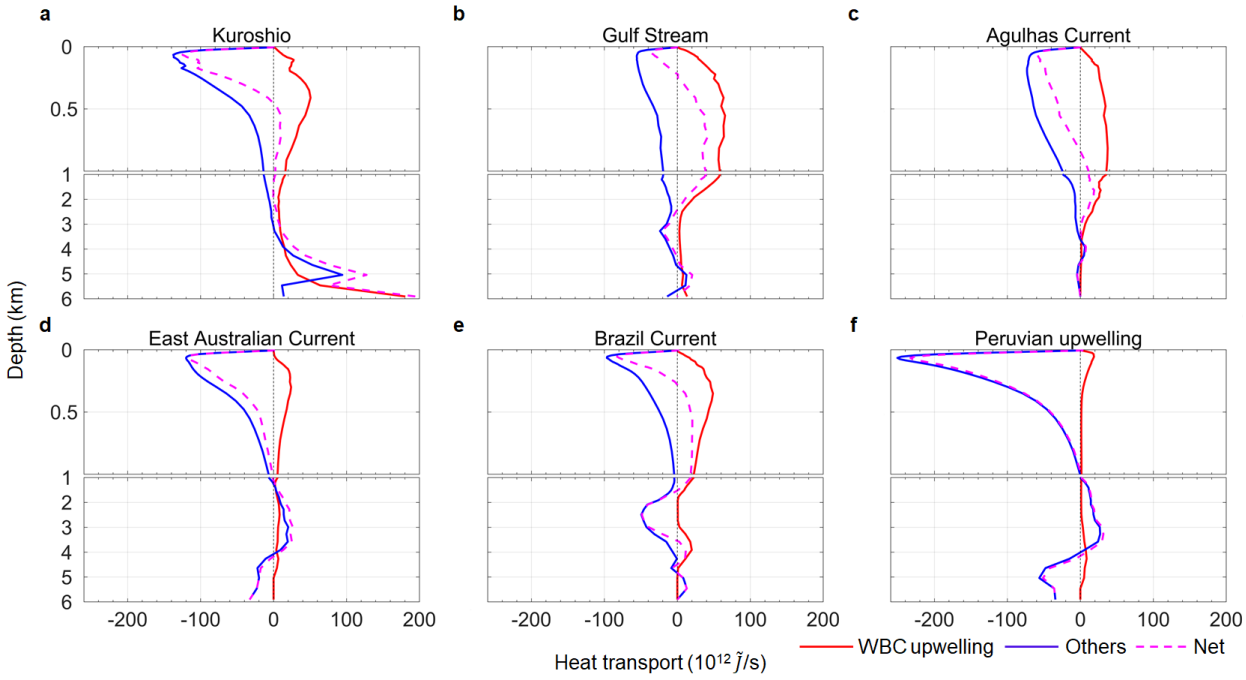

544

545 **Supplementary Fig. 10** Vertical heat transport in the WBC regions and Peruvian upwelling

546 region. **a** Kuroshio. **b** Gulf Stream. **c** Agulhas Current. **d** East Australian Current. **e** Brazil

547 Current. **f** Peruvian upwelling. $\tilde{J}$ means equivalent joules as we used normalized temperature at

548 each layer to calculate the heat flux. The results are based on ECCO.

549

550

551

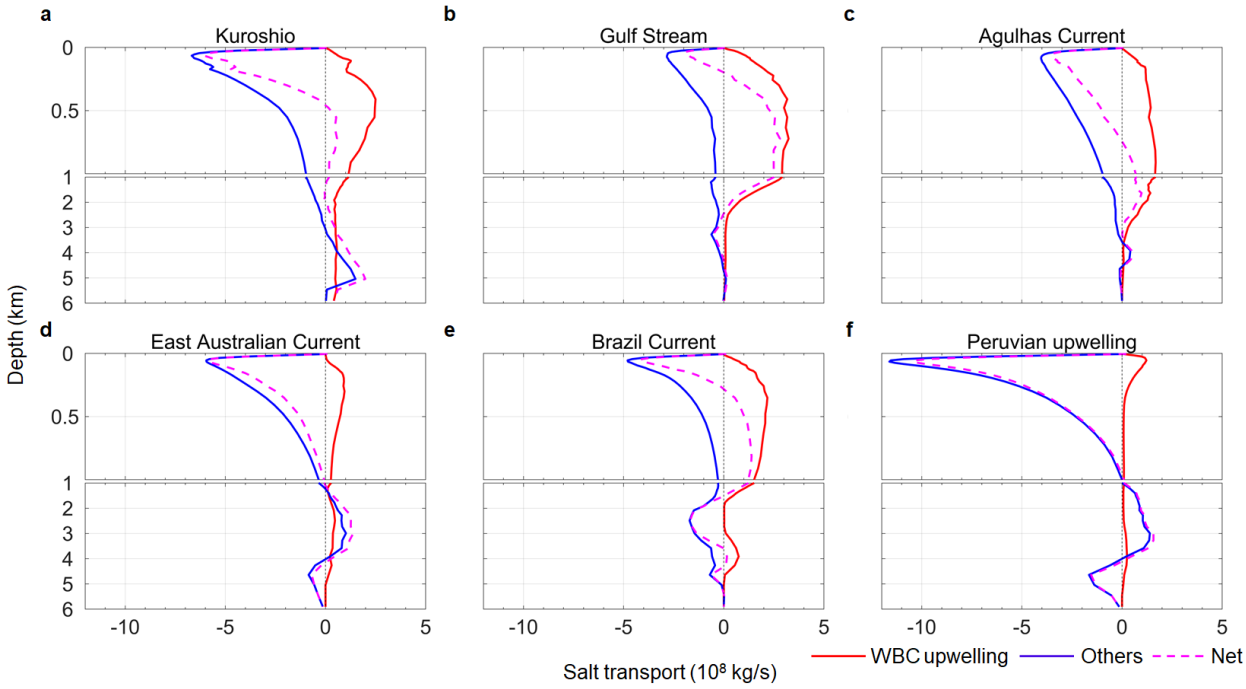

552

553 **Supplementary Fig. 11** Vertical salt transport in the WBC regions and Peruvian upwelling

554 region. **a** Kuroshio. **b** Gulf Stream. **c** Agulhas Current. **d** East Australian Current. **e** Brazil

555 Current. **f** Peruvian upwelling. The results are based on ECCO.

556

557

558

559

Supplementary Table

Supplementary Table 1: Summary of the six ocean data products

Product	ECCO	ECDA	ECMWF	GODAS	SODA	OFES
Version	v4r3		ora-s3		3.4.2	
Model	MITgcm	MOM4	HOPE	MOM3	POP2	MOM3
Lon grids	720	360	360	360	720	3600
Lat grids	360	200	179	418	330	1500
Vertical grids	50 (z^*)	50 (z)	29 (z^*)	40 (z^*)	50 (z^*)	54 (z)
Assimilated data	T, S, SST, SSS, SSH, OBP	T, S, SST	T, S, SSH	T	T, S, SST	
Time span	1992-2015	1961-2016	1959-2009	1980-2019	1980-2018	1950-2016

Lon means longitude; Lat means latitude; z in the vertical grid row means the vertical coordinate is in z level and z^* means z-star level; T means temperature; S means salinity; SST means sea surface temperature; SSS means sea surface salinity; SSH means sea surface height; OBP means ocean bottom pressure.